Multipolar Resonances with Designer Tunability Using VO_2 Phase-Change Materials

Jimmy John,[1] Yael Gutierrez,[2] Zhen Zhang,[3] Helmut Karl,[4] Shriram Ramanathan,[3] Régis Orobtchouk,[1] Fernando Moreno,[2] and Sébastien Cueff[1,*]

[1] *Institut des Nanotechnologies de Lyon-INL, UMR CNRS 5270, CNRS, Ecole Centrale de Lyon, 69134 Ecully, France*

[2] *Department of Applied Physics, Universidad de Cantabria, Avda. Los Castros s/n, 39005 Santander, Spain*

[3] *School of Materials Engineering, Purdue University, West Lafayette, Indiana 47907, USA*

[4] *Lehrstuhl für Experimentalphysik IV, Universität Augsburg, 86159 Augsburg, Germany*

(Received 20 December 2019; revised manuscript received 21 February 2020; accepted 17 March 2020; published 21 April 2020)

Subwavelength nanoparticles can support electromagnetic resonances with distinct features depending on their size, shape, and nature. For example, electric and magnetic Mie resonances occur in dielectric particles, while plasmonic resonances appear in metals. Here, we experimentally demonstrate that the multipolar resonances hosted by VO_2 nanocrystals can be dynamically tuned and switched thanks to the insulator-to-metal transition of VO_2. Using both Mie theory and Maxwell-Garnett effective-medium theory, we retrieve the complex refractive index of the effective medium composed of a slab of VO_2 nanospheres embedded in SiO_2 and show that such a resulting metamaterial presents distinct optical tunability compared to unpatterned VO_2. We further show that this approach provides a new degree of freedom to design low-loss phase-change metamaterials with record large figure of merit ($\Delta n/\Delta k$) and designer optical tunability.

DOI: 10.1103/PhysRevApplied.13.044053

I. INTRODUCTION

The potential of nanophotonics for tailoring light-matter interaction at the nanoscale has attracted considerable interest in recent years [1–3]. For example, metasurfaces enable an ultimate control of light fields thanks to abrupt phase modifications using engineered nanoscale elements [4,5]. A wealth of nanofabrication techniques are readily available to produce nanoscale elements with specific shapes, sizes, and nature. Thanks to these technological developments, light scattering by spherical nanoparticles revealed exciting optical phenomena such as strong localized optical resonances, directional scattering, or light emission control [6–9]. However, the dimensions of these nanoresonators, and the scale of nanophotonic devices make them difficult to tune and reconfigure. So, in essence, most nanophotonic devices are static devices. It is therefore currently a great challenge to find efficient means to dynamically tune photonic devices at the nanoscale [10,11].

Recently, a large number of researches make use of phase-change materials (PCM) to tune photonic devices. Although a large variety of PCMs exist, most of the works exploit the tunable properties of either VO_2 or (Ge, Sb)Te [12–15]. In the standard visible (vis) and near-infrared (NIR) ranges, these materials typically have large refractive-index modulation but also large extinction coefficients. So far, it has proven difficult to circumvent this extinction coefficient, which translates into net optical losses in photonic devices. One interesting approach to modify the intrinsic properties of these materials is to locally arrange or modify them by patterning, doping, or straining. These strategies were recently used to demonstrate phase modulation [16], tunable optical absorption [17,18], or switchable dielectric-plasmonic regimes [19]. A particularly promising method is to reduce the dimensions of VO_2 down to the nanoscale. This approach is not only interesting for gaining theoretical insights into the fundamentals of the insulator-to-metal transition (IMT) of VO_2 [20] but also to tailor the physical properties of this strongly correlated system. The first works on synthesis and characterization of VO_2 nanocrystals (NCs) were reported in 2002 [21,22], followed by studies on their nonlinear optical properties [23], and their potential for ultrafast modulation of optical transmission [24]. Recent works report various methods of fabrication of VO_2 nanocrystals and their use as thermochromic smart windows [25,26], differentially doped multilayer VO_2 films

*sebastien.cueff@ec-lyon.fr

[27], electrochemically induced transformations [28], or dynamical reconfiguration of optical devices [29–31].

Here, we show that an ensemble of VO_2 nanospheres support multipolar resonances and can be homogenized as a tunable effective-medium metamaterial whose optical properties and tunability are adjustable by design. Specifically, we exploit a Mie-theory-based extension of Maxwell-Garnett effective-medium approximation to precisely explain the light-matter interactions at play in VO_2 NCs and decompose it into multipolar modes. These multipolar resonances are both dynamically tunable through the IMT of VO_2 and adjustable via controlling the size of the particles. VO_2 NCs is therefore a tunable metamaterial platform whose properties can both be engineered through fabrication (size and density of VO_2 NCs) and actively tunable by external excitations (switching from insulator to metal). But more importantly, we show in the following that this metamaterial approach enables designing tunable composite metamaterials, presenting a refractive index modulation without induced extinction, or in other words a zero-induced extinction phase-change metamaterial.

II. OPTICAL PROPERTIES OF VO_2 THIN FILMS

VO_2 is a strongly correlated material that is dielectric at room temperature and becomes metallic when heated above 68 °C. According to band theory and given its crystallography, it should be metallic even at room temperature, but electron-electron correlations freeze the potential free carriers on their respective sites (Mott localization) [32–34]. Upon the transition, several interrelated physical processes occur: the crystallographic lattice changes from monoclinic to tetragonal (Peierls distortion), hence modifying the band structure and "liberating" free carriers. VO_2 therefore undergoes large changes in its electrical properties and its band structure, which translates into large modulation of its optical properties.

We investigate the optical properties of a thin layer of VO_2 across the IMT using spectroscopic ellipsometry combined with a heat cell (more details in Section 1 of the Supplemental Material [35]). Thanks to a physically consistent optical model (more details in the Supplemental Material [35]), we extract the dielectric function of VO_2 as a function of temperature. In Fig. 1, we show the complex optical permittivity of VO_2 upon phase change. As displayed in the figure, we see very large modifications of both the real (ϵ_1) and imaginary parts (ϵ_2) of the permittivity upon the IMT of VO_2.

The extraordinary feature of VO_2 is the strong modulation of its electric permittivity, which is as large as $\Delta\epsilon \sim 20$ in the near-infrared range. But, as explained previously, this modulation is accompanied by an intrinsic very large increase of the optical absorption, which dominates the optical response in the infrared range [36,37]. Given this large absorption, VO_2 is therefore often used as an on-off switch and little to no works actually make use of its refractive-index tunability.

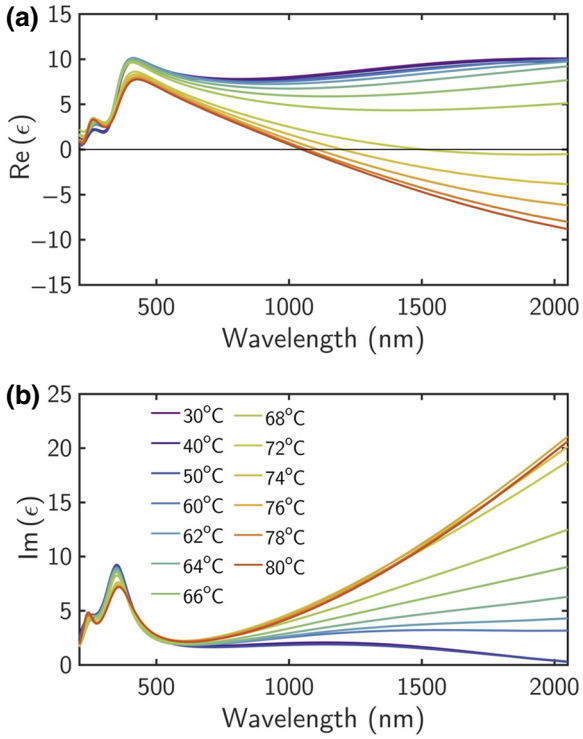

FIG. 1. Real and imaginary parts of the electric permittivity ϵ of a VO_2 thin film in the vis and NIR range as a function of temperature.

III. VO_2 NANOCRYSTALS

When an object is illuminated by an electromagnetic wave, it reradiates parts of the energy while being lost from the original wave. This phenomenon is known as scattering. The quantity and direction of light that is scattered depend on the nature, shape, and size of the object [38]. The problem becomes substantially more complex when the size of the object approaches the wavelength of the incident wave. In that situation, we can no longer assume the field to be constant in the object and the so-called "long-wavelength approximation" no longer holds, so retardation effects must be considered. To compute the scattered field, one needs a numerical approach for an arbitrary object. Such a complex problem can however be simplified if the object is a sphere. In 1908, Mie found an exact solution to that problem, by calculating the scattered field as a series solution [39]. The general idea is to expand the electric and magnetic fields in vector spherical harmonics. The field functions are then linear combinations of terms that are products of separable functions of the three spherical coordinates. The electromagnetic interaction of light with spheres can then be modeled following the Lorenz-Mie formalism for scattering and absorption

of light by small particles [40]. Within this formalism, the extinction, scattering, and absorption efficiencies are given by

$$Q_{\text{ext}} = \frac{2}{x^2}\sum_{n=1}^{\infty}(2n+1)\,\text{Re}(a_n + b_n), \tag{1}$$

$$Q_{\text{sca}} = \frac{2}{x^2}\sum_{n=1}^{\infty}(2n+1)(|a_n|^2 + |b_n|^2), \tag{2}$$

$$Q_{\text{abs}} = Q_{\text{ext}} - Q_{\text{sca}}, \tag{3}$$

where a_n and b_n are the so-called scattering coefficients [40]. These depend on both the particle optical properties (relative to its surrounding medium) and size. The size parameter x is defined as $x = 2\pi m_{\text{med}}R/\lambda$, where m_{med} is the refractive index of the surrounding medium, λ the wavelength of the incident light in vacuum, and R the sphere's radius. Physically, a_n and b_n are the weighting factors of the different excited electric and magnetic multipolar contributions. For instance, a_1 and b_1 represent the electric and magnetic dipolar modes, and a_2 and b_2 correspond to the electric and magnetic quadrupolar modes, respectively.

Figure 2 shows the absorption cross section Q_{abs} of a VO_2 sphere of radius 50 nm in its insulating and metallic states embedded in quartz ($m_{\text{med}} = 1.45$ for $\lambda = 1\ \mu$m [41]). Colored lines represent dipolar electric a_1, dipolar magnetic b_1, quadrupolar electric a_2, and quadrupolar magnetic b_2 contributions to Q_{abs}. It can be seen that, regardless of the state of VO_2, below 700 nm the electromagnetic response is dominated by the dipolar electric (DE) and magnetic response (DM), with a small contribution of the quadrupolar electric term (QE). These resonances correspond to whispering gallery modes [WGM, $\text{Re}(\epsilon) > 0$], which resonate at suitable wavelengths, and the magnetic resonance redshifted with respect to the electric one [8]. On the other hand, when VO_2 is in its metallic phase [$\text{Re}(\epsilon) < 0$], a DE localized surface-plasmon resonance (LSPR) appears at a longer wavelength (1015 nm). The higher the temperature, consequently, with increasing metallic character, the more intense the resonance. This resonance is plasmonic and its physical origin is the negative value of the dielectric constant above 1000 nm in the metallic phase.

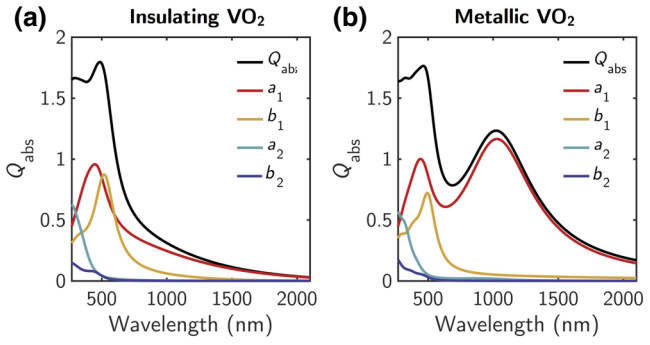

FIG. 2. Calculated absorption efficiency of VO_2 spheres with radius 50 nm in its (a) insulating and (b) metallic states embedded in quartz. Colored lines represent the dipolar electric a_1 (red), dipolar magnetic b_1 (yellow), quadrupolar electric a_2 (light blue), and quadrupolar magnetic b_2 (dark blue) contributions to Q_{abs}.

An ensemble of VO_2 nanospheres therefore enables a dynamic tuning of multipolar resonances together with their coherent effects for directionality purposes [42] and to actively control the presence and intensity of a plasmonic mode in the NIR.

IV. FABRICATION AND OPTICAL CHARACTERIZATION

The synthesis of a dense layer of isolated VO_2 nanocrystals embedded in about 100 nm depth below the surface begins with a high-fluence ion implantation of V^+ and O^+ with energies of 100 and 36 keV, respectively. These energies are chosen to produce overlapping concentration depth profiles of the elements. The formation of the VO_2 chemical compound is controlled by the fluence ratio of V to O (i.e., 8×10^{16} cm^{-2} to 1.6×10^{17} cm^{-2} and 4×10^{16} cm^{-2} to 8×10^{16} cm^{-2} for a ratio of 1:2). Then, ion-implantation nanocrystal growth is initiated by a rapid thermal-annealing (RTA) step at 1000 °C for 10 min in an inert gas at atmospheric pressure. After these steps, spherical VO_2 NCs are formed, embedded below the surface (for more details, see, e.g., [30]). As verified by TEM analysis [see Fig. 3(a)], the produced sample contains an ensemble of VO_2 nanospheres that are close to being perfectly spherical [31].

Unpatterned VO_2 thin films are fabricated as follows: 25 nm VO_2 is deposited on quartz substrate by magnetron sputtering. A V_2O_5 target is sputtered at a power of 100-W radio frequency. During deposition, the substrate is maintained at 750 °C; the chamber pressure is kept as 5 mtorr with flowing of 49.5 sccm Ar and 0.5 sccm 10% Ar-balanced oxygen gases.

Following the depositions, the analysis of the complex dielectric functions of all the samples of VO_2 (both NCs and thin films) are carried out using a variable-angle spectroscopic ellipsometer (UVISEL Horiba Jobin-Yvon). The incident broadband light source (Xenon) is polarized at 45°. After reflection off the sample under study, the light is directed to a spectrometer, dispersed by appropriate gratings and measured with UV-vis and NIR detectors. In the case of phase-modulated ellipsometer, like the one we use, we do not measure the ellipsometric angles Ψ and Δ directly. Instead, we measure I_s and I_c which, under our measurements conditions, are defined as follows: $I_s = \sin(2\Psi)\sin(\Delta)$ and $I_c = \sin(2\Psi)\cos(\Delta)$. The acquired ellipsometric parameters I_s and I_c of the samples are collected for varying angles 55°–70° over a spectral range

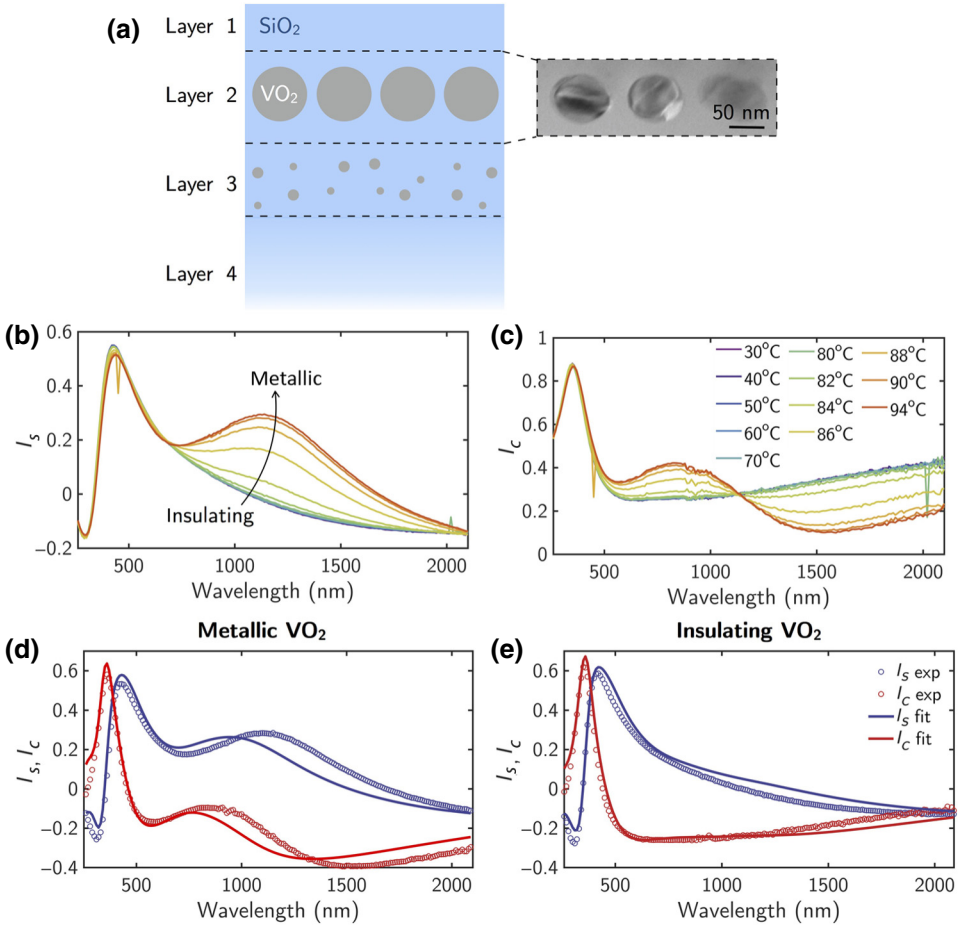

FIG. 3. (a) Sketch representing a cross-section view of the VO_2 NCs implanted in SiO_2 together with a TEM image of the VO_2-NC layer. (b),(c) Spectroscopic ellipsometry measurements of VO_2 NCs: (b) I_s parameter and (c) I_c parameter, both measured as a function of temperature (incident angle: 65°). (d),(e) Fitting (solid line) and experimental measurements (circles) of the ellipsometric parameters I_s (blue) and I_c (red) for both states of VO_2 NCs: (d) metallic and (e) insulating. (Incident angle of 55° is displayed here for a better clarity of the superimposed I_s and I_c parameters.)

of 260–2100 nm. The complex dielectric functions of samples and their thicknesses can be derived by fitting realistic optical models to these experimental data (more details in the Supplemental Material [35]). To analyze temperature-dependent optical properties, the acquisitions are carried out in a range of temperatures from 30 to 80 °C using a digitally controlled heat cell (Linkam THMSEL350V).

In the following, we present our ellipsometric measurements and analysis via these functions I_s and I_c, that are directly related to the usual ellipsometry angles Ψ and Δ. Figures 3(b) and 3(c) show the evolution of the I_s and I_c parameters of ellipsometry measurements as a function of temperature, the effect of the IMT of VO_2 NCs is clearly observable on the raw ellipsometry measurements, with the appearance of a large peak in I_s whose intensity progressively increases around 1100 nm. This phenomenon is reversible, with a broad hysteresis behavior (more details in the Supplemental Material [35]), and is a clear signature of the presence of stoichiometric VO_2 in the sample.

V. RETRIEVAL OF THE EFFECTIVE PARAMETERS OF THE METAMATERIAL

We now want to retrieve the effective permittivity of the active layer containing VO_2 NCs. From previous TEM analysis [31], we know that the VO_2 NCs medium is a single plane of NCs that are spaced by a few tens of nanometers. In order to model the optical response of the slab composed of VO_2 NCs embedded in quartz, we calculate its effective refractive index m_{eff} using a Mie-theory-based extension of Maxwell-Garnett effective-medium approximation, as proposed by Doyle [43,44]. Using this approach, we can calculate an effective electric permittivity (ϵ_{eff}) and magnetic permeability (μ_{eff}) that are directly governed by the Mie dipolar electric a_1 and magnetic b_1 dipolar coefficients, respectively. In this way, we take into account size effects that are ignored by the electrostatic approximation, which is the base of conventional Maxwell-Garnett effective-medium approximation. The dipolar coefficients are enough to model the response of the VO_2 particles since the quadrupolar terms are negligible as seen in Fig. 1. Therefore, ϵ_{eff} and μ_{eff} can be written as

$$\epsilon_{\text{eff}} = \frac{x^3 + 3ifa_1}{x^3 - \frac{3}{2}ifa_1}, \tag{4}$$

$$\mu_{\text{eff}} = \frac{x^3 + 3ifb_1}{x^3 - \frac{3}{2}ifb_1}, \tag{5}$$

where x is the size parameter of the VO_2 spheres and f the volume filling fraction of the VO_2 spheres in the slab [the complete derivation for Eqs. (4) and (5) can be found in the Supplemental Material [35]]. From the values of ϵ_{eff} and μ_{eff} the effective complex refractive index of the slab can be calculated as

$$m_{\text{eff}} = n_{\text{eff}} + ik_{\text{eff}} = \sqrt{\epsilon_{\text{eff}}.\mu_{\text{eff}}}. \tag{6}$$

In the following, we fit the experimental ellipsometry measurements with a multilayer model composed of four layers as sketched in Fig. 3(a): (i) a thin SiO_2 layer, (ii) the VO_2 NCs + SiO_2 effective layer, (iii) an intermediate layer containing vanadium inclusions and impurities, and (iv) a semi-infinite SiO_2 substrate. This four-layer model is justified by TEM observations of the sample's cross sections. Indeed, from previous TEM analysis on similar samples, we know that the implantation process of V^+ and O^+ ions produces a layer of almost perfectly spherical VO_2 nanocrystals (layer 2), but also another layer below containing very small (<10 nm) metallic vanadium inclusions (layer 3), as found by elemental composition measurements [45]. We use a reference dispersion file for SiO_2 (Palik [46]). The respective thicknesses of SiO_2 top layer, VO_2-NC layer and V inclusion layer are set as free fit parameters. None of the material's dispersion are fit, rather we modify the size and density of VO_2 NCs in our Mie-Maxwell-Garnett model to adjust the fits to the measurements. Thin partially absorbing films are known to present correlations between thickness and dispersion, which make the ellipsometry analysis difficult. Interestingly, this situation becomes manageable when measuring thin films of PCMs: their optical dispersion is modulated across the change of phase, while their thickness remains the same (this is especially true for VO_2, for which there is no change of thickness upon the insulator-to-metal transition). This phenomenon was previously used to find unique solutions for the ellipsometry fit of thin films of VO_2 [37]. We follow the same method for our VO_2-NC layer: to break the correlations between thickness and complex refractive index, we simultaneously fit the ellipsometry measurements of VO_2 NCs in both their insulating and metallic state and we force the final fitted thickness to converge towards the same value in both states of VO_2. In other words, the final fit yields the same thicknesses for the different layers whatever the phase of VO_2 NCs. The only difference between the two models for VO_2 insulating and metallic lies in the dispersion of VO_2 NCs.

In Figs. 3(d) and 3(e), we show the optimized fits together with the experimental data. We obtain an overall good correspondence between model and measurements for a VO_2-NC size of $R = 35$ nm and a filling factor $f = 0.18$. Based on our different fits to the experimental measurements, we can give an estimated uncertainty for the extracted values for the sizes and filling factor of VO_2 NCs to about 5%. If we round up this number, the extracted values with their associated uncertainties are $R = 35\text{ nm} \pm 2\text{ nm}$ and $f = 0.18 \pm 0.01$.

The fits are nearly perfect in the UV-vis range but a slight discrepancy appears in the NIR. The observed discrepancy in Figs. 3(d) and 3(e) between the model and the experimental results is due to different effects, which cannot be included without losing simplicity in the proposed model. The two most important are the electromagnetic interaction between the particles and a potentially non-negligible degree of polydispersity in the size distribution of the VO_2 NCs. The electromagnetic interaction between nanoparticles has a long-standing history and a nice work on this effect can be found in Rechberger *et al.* [47]. We apply the results of this research to our case and the details can be found in the Supplemental Material [35]. Here, we consider the experimental conditions used in the ellipsometry measurements with an exciting beam linearly polarized at 45° with respect to the incidence plane. In the metallic phase, the pure plasmonic resonance is affected by blue and red shifts due to the interparticle electromagnetic interaction with a clear net red shift of this resonance. This explains the apparent discrepancy observed between the measured spectral position of the plasmonic peak around 1000 nm and that predicted with our model where multiple interactions are not included. Concerning the insulating phase, its resonance is clearly less influenced by electromagnetic interaction between the particles. It is important to point out that this resonance is composed mainly of two dipolar ones (see Fig. 1) of electric and magnetic character, respectively. As shown in the Supplemental Material [35], due to the particle interaction, there is a competition between the blue shift undergone by the magnetic contribution and the red shift for the electric one [48]. The net result is a slight blue shift of the whole resonance when the interparticle gap is small. This is the small discrepancy we observe in Fig. 3 when the experiment and the model result are compared for the resonance at 380 nm.

Concerning polydispersity, some detailed calculations have been included in the Supplemental Material [35] but the main conclusion is that, assuming an asymmetric size distribution, the net effect will be a general red shift and broadening of the resonance peak, especially for those resonances of low energy (long wavelengths) and associated to the metallic phase, which are more sensitive to changes in the morphology and optical properties of the VO_2 nanoscatterers.

Other effects can also present minor contributions to the discrepancies observed in Figs. 3(d) and 3(e). Indeed, we approximate VO_2 NCs as composed of purely stoichiometric VO_2 and we neglect the presence of suboxides such as V_2O_5 at the NC surface. Furthermore, we directly used the dispersion as extracted from VO_2 thin-film measurements to compute the different Mie coeffients. By doing so, we made the hypothesis that the complex

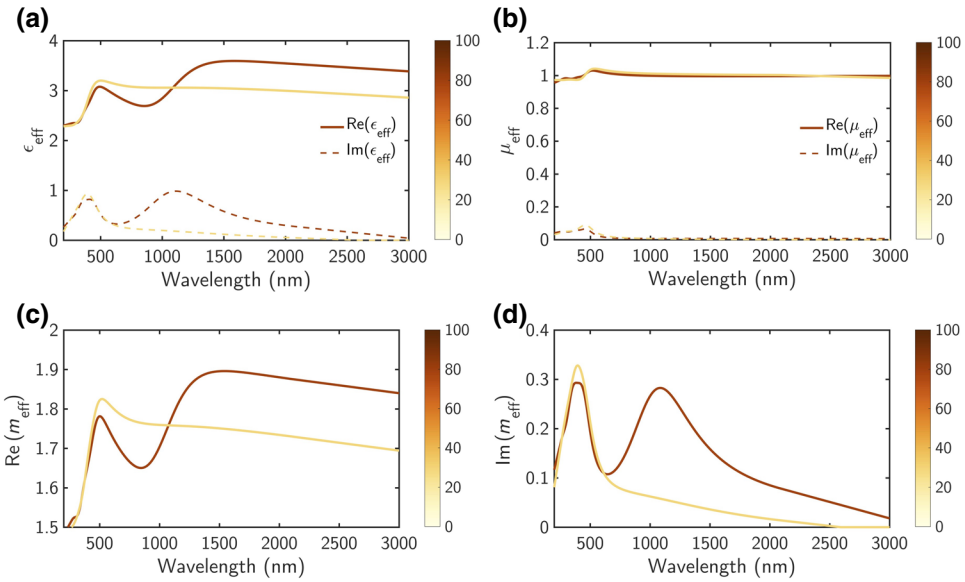

FIG. 4. (a) Effective dielectric function (ϵ_{eff}), (b) magnetic permeability (μ_{eff}), and (c) real and (d) imaginary parts of the effective refractive index ($m_{\text{eff}} = n_{\text{eff}} + ik_{\text{eff}}$) of a slab of quartz with VO_2 spheres with radius $R = 35$ nm and a filling fraction $f = 0.18$ in their insulating (low-temperature) and metallic (high-temperature) states.

permittivity of VO_2 inside the NCs has the exact same dispersion as VO_2 thin films, which could be subject to discussions [20].

Even though we make all these approximations and neglect potential interactions in the fits, we find a remarkably good qualitative agreement between measurements and calculations. Furthermore, this good agreement holds for all angles of incidence used in this study ($55^\circ - 70^\circ$). We emphasize that this simple model is able to reproduce well the prominent features of the optical response for both states of VO_2 by simply changing the dispersion of VO_2 from insulating to metallic. Indeed, the calculations nicely reproduce the first peak in the visible, which is a combination of electric and magnetic dipole resonances and the second peak in the NIR, which is a plasmonic resonance. The latter is only present when the VO_2 is metallic, e.g., when the real part of the permittivity is negative and is therefore a dynamically tunable resonance.

These calculations enable us to retrieve the effective permittivity of the active VO_2-NC layer and homogenize it as an effective metamaterial medium. Figures 4(a)–4(d) show the calculated ϵ_{eff}, μ_{eff}, and m_{eff} for a slab with VO_2 spheres with radius $R = 35$ nm and a filling fraction $f = 0.18$ in their insulating (low-temperature) and metallic (high-temperature) states. These retrieved ϵ_{eff} and μ_{eff} values are effective angle-independent metamaterial parameters, describing the global optical properties of the hybrid medium.

We see clear differences in the optical dispersion as compared to unpatterned VO_2 layer. In particular, there are ranges of wavelength for which the IMT of VO_2 produces a large modulation of n_{eff} with a simultaneously low k_{eff} that is much lower than in bulk VO_2. This is especially true in the NIR, for which k_{eff} remains lower than 0.1.

VI. DISCUSSION

We show that the main spectral characteristics of VO_2-NC-based metamaterials can be calculated using a combination of Mie theory and Maxwell-Garnett effective medium. From there, we can now predict the expected optical properties of VO_2 NCs of arbitrary sizes. In the following, we show how this framework can be used to design tunable metamaterials with tailored properties in desired wavelength ranges. Figures 5(a)–5(d) show the calculated evolution of the n_{eff} and k_{eff} values of VO_2 NCs in both their insulating and metallic states for different diameters of NCs.

In the insulating state, the absorption peaks are controlled by the Mie resonances while in the metallic state they are dominated by the plasmonic resonance. We can directly see that, by adjusting the size of NCs, we control the spectral position of the absorption peaks in both the insulating and metallic states [see Figs. 5(b) and 5(d)]. The size of the VO_2 NCs therefore enables tailoring the spectral distribution of the multipolar resonances hosted by this metamaterial.

To have a more general picture of the different regimes of tunability we can obtain with this system, Figs. 5(e) and 5(f) display the amplitude of refractive-index modulation produced by the IMT of VO_2 as a function of NC size. To do so, we plot Δn_{eff} and Δk_{eff}, which are defined as $\Delta n_{\text{eff}} = n_{\text{eff,insulating}} - n_{\text{eff,metallic}}$ and $\Delta k_{\text{eff}} = k_{\text{eff,insulating}} - k_{\text{eff,metallic}}$ and which represent the amplitude of modulation of the effective refractive index and extinction coefficient, respectively. With this figure, we can pinpoint specific regions of the size versus wavelength map in which the switching of VO_2 either translates into a tunable refractive index or a tunable extinction coefficient.

Interestingly, by plotting the Δn_{eff} and Δk_{eff} values calculated for a few selected VO_2-NC sizes (as displayed

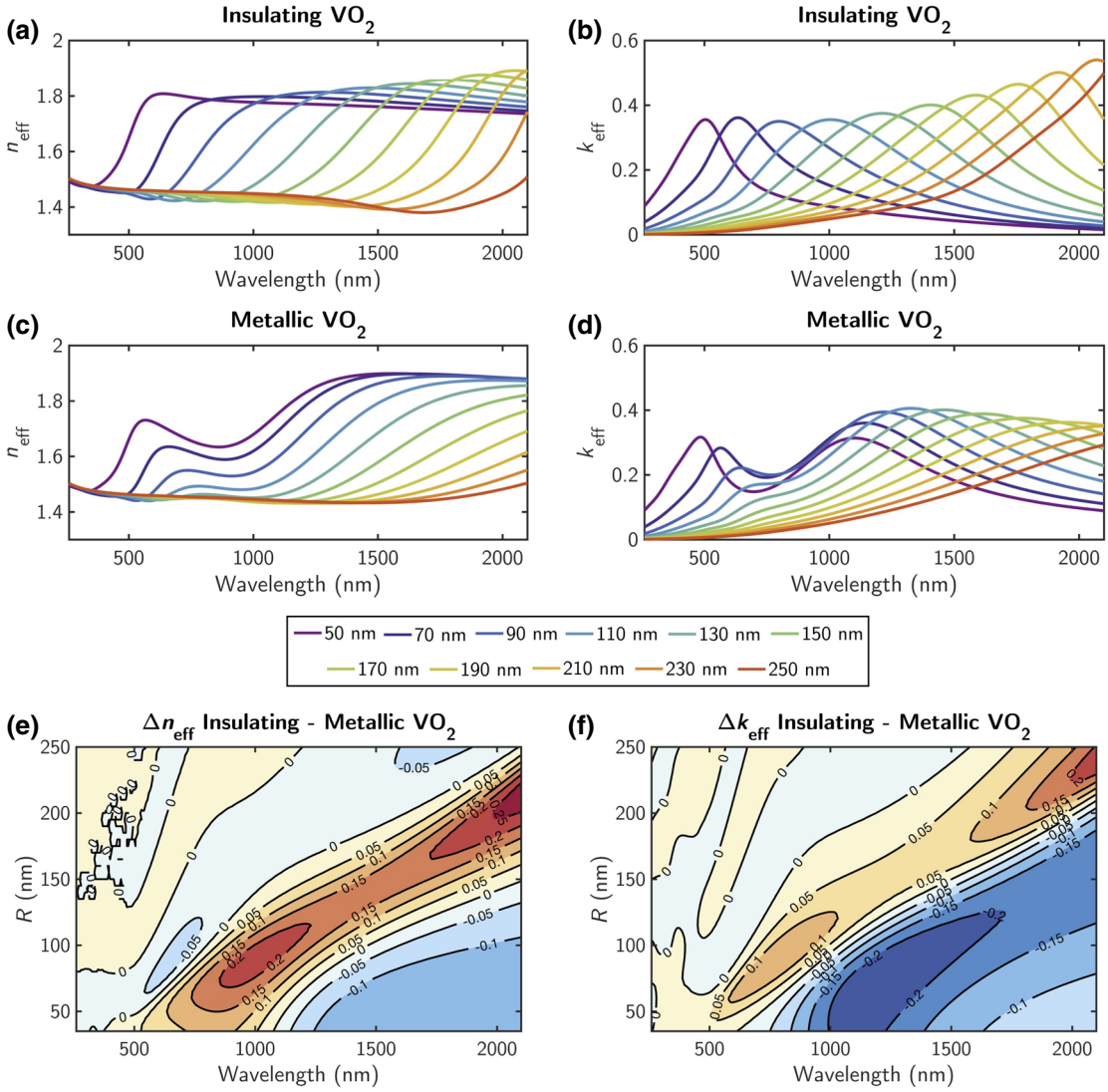

FIG. 5. Variation of effective optical parameters for different sizes of nanocrystals in both states of VO_2. (a),(b) n_{eff} and k_{eff} for insulating VO_2 with a filling fraction $f = 0.18$. (c),(d) n_{eff} and k_{eff} for metallic VO_2. (e),(f) The amplitude of modulation of the effective refractive index of the metamaterial as a function of NC size. (e) Δn_{eff} and (f) Δk_{eff}.

in Fig. 6), we immediately see that around the maximum Δn_{eff} reached for each NC size, we simultaneously have $\Delta k_{\text{eff}} = 0$. Furthermore, the wavelength at which this effect is obtained is directly governed by the size of VO_2 NCs. In other words, this phase-change metamaterial platform enables tailoring a dynamical tuning of refractive index without modifying the optical absorption. As displayed in Fig. 6, this "zero-induced-extinction" refractive-index tuning occurs in a designer wavelength range via selecting an appropriate size of NC.

By plotting the figure of merit (FOM) $\Delta n_{\text{eff}}/\Delta k_{\text{eff}}$ for different sizes of NCs and comparing the obtained FOM to the corresponding one for VO_2 thin films, we immediately see that not only the FOM is enhanced by more than 2 orders of magnitude but we can design the system to select the wavelength at which the FOM is boosted via the size of VO_2 NCs. This designer high FOM is much larger than in any other existing "unpatterned" PCMs [49], and highlights the usefulness of our metamaterial approach. We also note that the opposite effect can be exploited, namely, close to the maximum Δk_{eff}, we can simultaneously have negligible Δn_{eff}. So this platform can be used to actively control the absorption without modifying the refractive index of the medium (e.g., for $R = 95$ nm at $\lambda = 1500$ nm we get $\Delta k_{\text{eff}} = -0.2$ and $\Delta n_{\text{eff}} = 0$).

We envision another exciting opportunity for this metamaterial as an active platform to control scattering properties and directional beaming of light. Indeed, when multipolar resonances are spectrally overlapping in nanoparticles, the scattered fields can interfere and produce directional scattering. In particular, spectrally overlapping DE and DM resonances yield the so-called Kerker

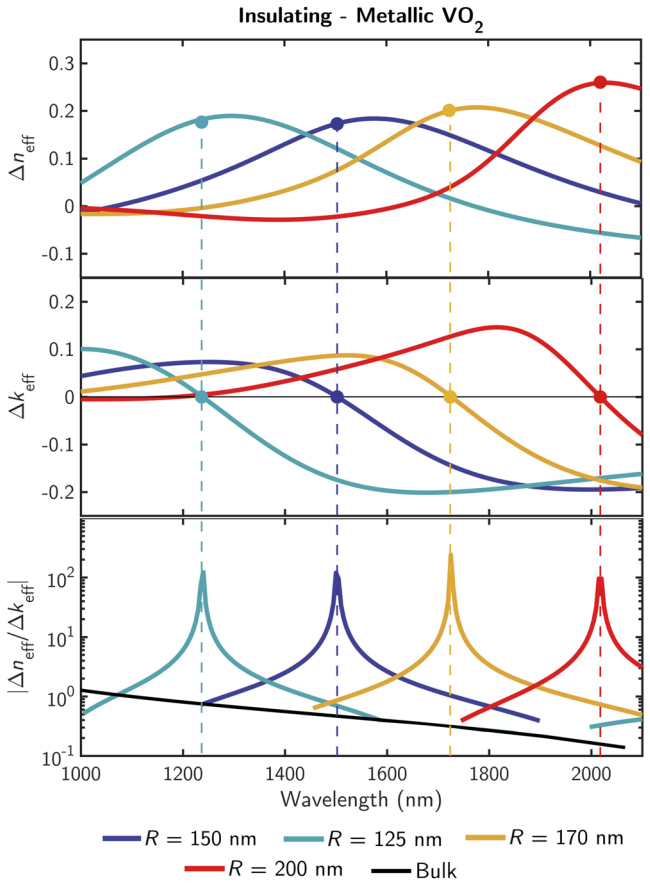

FIG. 6. Spectral variation of the amplitude of modulation of the effective refractive index (Δn_{eff} and Δk_{eff}) of the metamaterial for selected NC size. Bottom graph: figure of merit (FOM $= \Delta n_{\text{eff}}/\Delta k_{\text{eff}}$) of the VO_2-NC platform for different sizes of nanocrystals and compared to the FOM for a VO_2 thin film.

conditions that either suppress the forward or the backward scattering of light [8,50]. Figure 7 displays the multipolar decomposition of light fields within VO_2 NCs as a function of size and VO_2 phase, either insulating or metallic. We see that each size of NC produces overlapping DE and DM resonances, which coherently interfere at specific wavelengths. Then, when the VO_2 is switched from its insulating phase to the metallic one, we can suppress the DM contribution associated to the b_1 coefficient and strongly enhance the DE contribution associated to the a_1 coefficient.

In other words, at specific wavelengths we switch from a dielectric DM resonances to a plasmonic DE resonance. This implies that this hybrid metamaterial enables an active and dynamical control of the Kerker conditions [50]. From that perspective, we foresee a dynamic modulation of the directionality of light scattering as well as actively tunable perfect reflection or absorption. We also note the presence of tunable quadrupolar modes (a_2 and b_2 coefficients, Fig. 7) that may be used for complex tunable interference phenomena between different multipoles, hence opening a wealth of different possibilities of spatially distributing the scattered light for directionality control purposes (see [42,51] for more details). This tunable multipole can also find interest in the recently proposed framework of spontaneous emission engineering through intereferences between higher-order multipoles [52].

VII. CONCLUSION

We demonstrate that VO_2 NCs integrated in SiO_2 as spherical nanoinclusions enable exploiting the VO_2 IMT to tune and switch multipolar modes in the visible and near-infrared ranges. In particular, we show the presence of a plasmonic mode in the NIR whose gradual appearance and intensity are directly controlled by the VO_2 state. The presence of two simultaneous dipole resonances in two different spectral regions, vis and NIR, could open the possibility of new "multiplexing"-based techniques for SERS applications. Contrary to bulk and thin-film VO_2, such a metamaterial approach provides means to tailor the complex refractive index and tunability of phase-change materials. Indeed, we show that, by adjusting the VO_2-NC size, this system can be exploited as a designer phase-change metamaterial with adjustable refractive-index modulation and absorption modulation. In particular, we can design the system to have a large refractive-index tunability without

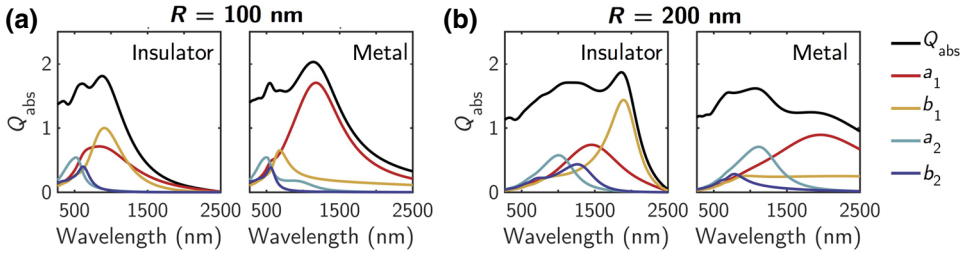

FIG. 7. Calculated absorption cross-section efficiency Q_{abs} of NCs of different sizes in their insulator and metallic states embedded in quartz. Colored lines represent the dipolar electric a_1 (red), dipolar magnetic b_1 (yellow), quadrupolar electric a_2 (light blue), and quadrupolar magnetic b_2 (dark blue) contributions to Q_{abs}.

inducing modulation of the extinction coefficient at specific wavelengths. This zero-induced-extinction refractive-index tuning opens up new regimes of very large FOM that are unattainable with conventional unpatterned PCMs layers. Furthermore, such VO_2 NCs can be optically switched at femtosecond timescale (approximately 150 fs) [24] and present very large hysteresis (see [30] and the Supplemental Material [35]). We can therefore envision this platform to be used for ultrafast all-optical integrated systems with memory effects. Note however that the speed of modulation is ultimately limited by the fall times for VO_2 devices, which typically depends on device dimensions, thermal dissipation, ambient temperature, and actuation mechanism [53,54]. Reaching the sub-nanosecond regime requires optimizing the optical and thermal environment of nanostructures for heat management.

Compared to other methods of nanopatterning PCMs, we emphasize that the resulting metamaterial presents several benefits from a practical point of view, and most notably the nanostructures are embedded in a dielectric host that protects them from the environment and consequent processes that can affect its optical response (protection from oxidization [55], chemical reaction [56], mechanical scratches,...). This makes such a platform extremely easy to handle and to integrate in various environments, contrary to thin films of phase-change materials that are very sensitive.

The samples presented here are fabricated by ion implantation, a technique that is widely used in the microelectronics industry and can therefore be exploited for large-scale fabrication of samples. Furthermore, the size, density, and depth of NCs in the host can be controlled through adjustment of implantation parameters and annealing process. This implantation process can be carried out in many different CMOS-compatible platforms such as thermal SiO_2 on silicon substrate and results in a flat surface that does not require any complex postprocess step such as CMP to planarize the device. A next logical step is to integrate nanophotonic devices on top of this metamaterial for a wealth of tunable functionalities such as an active control of spontaneous light emission [9,52,57] or dynamically tunable Huygen's metasurfaces [58].

From a broader scientific perspective, the results presented here help define an alternative system with which to study tunable interactions between nanoparticles and tunable interferences between multipolar resonances leading to interesting scattering directional properties. Our research shows that there are real materials [other than Si as a typical example of high refractive index material (see Refs. [7] and [8])] with phase-change properties that support the study made in Ref. [42]. With VO_2 nanocrystals, the analyzed directionality properties are tunable by taking advantage of its phase-change properties. This is a practical tunability where we can keep both NP size and exciting wavelength fixed. In the basic research of Ref. [42], the tunability is obtained by changing the wavelength or the size of the particle (size parameter tunability) to see a change in the directionality, which many times is unpractical. As a result, our research serves as a testbed for dynamical modulation of light scattering, tunable Kerker effects, and active control of light directionality.

ACKNOWLEDGMENTS

This work is partly supported by the French National Research Agency (ANR) under the project SNAPSHOT (ANR-16-CE24-0004). F.M. thanks the Ministerio de Ciencia, Innovación y Universidades for its support under project PGC2018-096649-B-100. Y.G. thanks the University of Cantabria for her FPU grant. Z.Z. and S.R. acknowledge AFOSR FA9550-18-1-0250 for support. The authors thank Professor David E. Aspnes for helpful discussions.

J.J. and Y.G. contributed equally to the Paper.

[1] L. Novotny and B. Hecht, *Principles of Nano-Optics* (Cambridge University Press, New York, 2012).

[2] A. F. Koenderink, A. Alu, and A. Polman, Nanophotonics: Shrinking light-based technology, Science **348**, 516 (2015).

[3] Y. Kivshar and A. Miroshnichenko, Meta-optics with Mie resonances, OPN **28**, 24 (2017).

[4] H.-T. Chen, A. J. Taylor, and N. Yu, A review of metasurfaces: Physics and applications, Rep. Prog. Phys. **79**, 076401 (2016).

[5] N. Yu and F. Capasso, Flat optics with designer metasurfaces, Nat. Mater. **13**, 139 (2014).

[6] K. L. Kelly, E. Coronado, L. L. Zhao, and G. C. Schatz, The optical properties of metal nanoparticles: The influence of size, shape, and dielectric environment, J. Phys. Chem. B **107**, 668 (2003).

[7] A. García-Etxarri, R. Gómez-Medina, L. S. Froufe-Pérez, C. López, L. Chantada, F. Scheffold, J. Aizpurua, M. Nieto-Vesperinas, and J. J. Sáenz, Strong magnetic response of submicron silicon particles in the infrared, Opt. Express **19**, 4815 (2011).

[8] J. Geffrin, B. García-Cámara, R. Gómez-Medina, P. Albella, L. Froufe-Pérez, C. Eyraud, A. Litman, R. Vaillon, F. González, M. Nieto-Vesperinas, J. Sáenz, and F. Moreno, Magnetic and electric coherence in forward- and back-scattered electromagnetic waves by a single dielectric subwavelength sphere, Nat. Commun. **3**, 1171 (2012).

[9] S. Bidault, M. Mivelle, and N. Bonod, Dielectric nanoantennas to manipulate solid-state light emission, J. Appl. Phys. **126**, 094104 (2019).

[10] C. Ferrera, N. Kinsey, A. Shaltout, C. DeVault, V. Shalaev, and A. Boltasseva, Dynamic nanophotonics, JOSA B **34**, 95 (2017).

[11] N. I. Zheludev, Obtaining optical properties on demand, Science **348**, 973 (2015).

[12] M. Wuttig, H. Bhaskaran, and T. Taubner, Phase-change materials for non-volatile photonic applications, Nat. Photonics **11**, 465 (2017).

[13] Y. Ke, S. Wang, G. Liu, M. Li, T. J. White, and Y. Long, Vanadium dioxide: The multistimuli responsive material and its applications, Small **14**, 1802025 (2018).

[14] R. Shi, N. Shen, J. Wang, W. Wang, A. Amini, N. Wang, and C. Cheng, Recent advances in fabrication strategies, phase transition modulation, and advanced applications of vanadium dioxide, Appl. Phys. Rev. **6**, 011312 (2019).

[15] S. Cueff, D. Li, Y. Zhou, F. J. Wong, J. A. Kurvits, S. Ramanathan, and R. Zia, Dynamic control of light emission faster than the lifetime limit using VO_2 phase-change, Nat. Commun. **6**, 8636 (2015).

[16] Y. Kim, P. C. Wu, R. Sokhoyan, K. A. Mauser, R. Glaudell, G. Kafaie Shirmanesh, and H. A. Atwater, Phase modulation with electrically tunable vanadium dioxide phase-change metasurfaces, Nano Lett. **19**, 3961 (2019).

[17] Z. Zhu, P. G. Evans, R. F. Haglund, Jr., and J. G. Valentine, Dynamically reconfigurable metadevice employing nanostructured phase-change materials, Nano Lett. **17**, 4881 (2017).

[18] J. Rensberg, S. Zhang, Y. Zhou, A. S. McLeod, C. Schwarz, M. Goldflam, M. Liu, J. Kerbusch, R. Nawrodt, and S. Ramanathan *et al.*, Active optical metasurfaces based on defect-engineered phase-transition materials, Nano Lett. **16**, 1050 (2016).

[19] N. A. Butakov, I. Valmianski, T. Lewi, C. Urban, Z. Ren, A. A. Mikhailovsky, S. D. Wilson, I. K. Schuller, and J. A. Schuller, Switchable plasmonic–dielectric resonators with metal–insulator transitions, ACS Photonics **5**, 371 (2017).

[20] L. Whittaker, C. J. Patridge, and S. Banerjee, Microscopic and nanoscale perspective of the metal- insulator phase transitions of VO_2: Some new twists to an old tale, J. Phys. Chem. Lett **2**, 745 (2011).

[21] R. Lopez, L. Boatner, T. Haynes, L. C. Feldman, and R. Haglund, Jr., Synthesis and characterization of size-controlled vanadium dioxide nanocrystals in a fused silica matrix, J. Appl. Phys. **92**, 4031 (2002).

[22] R. Lopez, T. Haynes, L. Boatner, L. C. Feldman, and R. Haglund, Jr., Size effects in the structural phase transition of VO_2 nanoparticles, Phys. Rev. B **65**, 224113 (2002).

[23] R. Lopez, R. F. Haglund, Jr., L. C. Feldman, L. A. Boatner, and T. E. Haynes, Optical nonlinearities in VO_2 nanoparticles and thin films, Appl. Phys. Lett. **85**, 5191 (2004).

[24] M. Rini, A. Cavalleri, R. W. Schoenlein, R. López, L. C. Feldman, R. F. Haglund, L. A. Boatner, and T. E. Haynes, Photoinduced phase transition in VO_2 nanocrystals: Ultrafast control of surface-plasmon resonance, Opt. Lett. **30**, 558 (2005).

[25] Y. Wei, H. Ebendorff-Heidepriem, and J. Zhao, Recent advances in hybrid optical materials: Integrating nanoparticles within a glass matrix, Adv. Opt. Mater. **7**, 1900702 (2019).

[26] B. Zhuang, Z. Dai, S. Pang, H. Xu, L. Sun, and F. Ma, 3D ordered macroporous VO_2 thin films with an efficient thermochromic modulation capability for advanced smart windows, Adv. Opt. Mater. **7**, 1900600 (2019).

[27] T. Paik, S.-H. Hong, E. A. Gaulding, H. Caglayan, T. R. Gordon, N. Engheta, C. R. Kagan, and C. B. Murray, Solution-processed phase-change VO_2 metamaterials from colloidal vanadium oxide (VO_x) nanocrystals, ACS Nano **8**, 797 (2014).

[28] C. J. Dahlman, G. LeBlanc, A. Bergerud, C. Staller, J. Adair, and D. J. Milliron, Electrochemically induced transformations of vanadium dioxide nanocrystals, Nano Lett. **16**, 6021 (2016).

[29] J. Zimmer, A. Wixforth, H. Karl, and H. J. Krenner, Ion beam synthesis of nanothermochromic diffraction gratings with giant switching contrast at telecom wavelengths, Appl. Phys. Lett. **100**, 231911 (2012).

[30] T. Jostmeier, J. Zimmer, H. Karl, H. J. Krenner, and K. Betz, Optically imprinted reconfigurable photonic elements in a VO_2 nanocomposite, Appl. Phys. Lett. **105**, 071107 (2014).

[31] T. Jostmeier, M. Mangold, J. Zimmer, H. Karl, H. J. Krenner, C. Ruppert, and K. Betz, Thermochromic modulation of surface plasmon polaritons in vanadium dioxide nanocomposites, Opt. Express **24**, 17321 (2016).

[32] A. Zylbersztejn and N. F. Mott, Metal-insulator transition in vanadium dioxide, Phys. Rev. B **11**, 4383 (1975).

[33] N. F. Mott, Metal-insulator transition, Rev. Mod. Phys. **40**, 677 (1968).

[34] M. Imada, A. Fujimori, and Y. Tokura, Metal-insulator transitions, Rev. Mod. Phys. **70**, 1039 (1998).

[35] See Supplemental Material at http://link.aps.org/supplemental/10.1103/PhysRevApplied.13.044053 for more details on the spectroscopic ellipsometry measurements, on the derivation of the expressions for effective permettivity and permeability and on the modelization of interactions between particles and polydispersity effects, which includes Refs. [59–63].

[36] C. Wan, Z. Zhang, D. Woolf, C. M. Hessel, J. Rensberg, J. M. Hensley, Y. Xiao, A. Shahsafi, J. Salman, S. Richter *et al.*, Optical properties of thin-film vanadium dioxide from the visible to the far infrared, Ann. Phys.-Berlin **531**, 1900188 (2019).

[37] J. Sun and G. K. Pribil, Analyzing optical properties of thin vanadium oxide films through semiconductor-to-metal phase transition using spectroscopic ellipsometry, Appl. Surf. Sci. **421**, 819 (2017).

[38] C. Noguez, Surface plasmons on metal nanoparticles: The influence of shape and physical environment, J. Phys. Chem. C **111**, 3606 (2007).

[39] G. Mie, Beiträge zur optik trüber medien, speziell kolloidaler Metallösungen, Ann. Phys. **330**, 377 (1908).

[40] C. F. Bohren and D. R. Huffman, *Absorption and Scattering of Light by Small Particles* (John Wiley & Sons, New York, NY, 2008).

[41] I. H. Malitson, Interspecimen comparison of the refractive index of fused silica, JOSA **55**, 1205 (1965).

[42] M. I. Tribelsky, J.-M. Geffrin, A. Litman, C. Eyraud, and F. Moreno, Small dielectric spheres with high refractive index as new multifunctional elements for optical devices, Sci. Rep. **5**, 12288 (2015).

[43] R. Ruppin, Evaluation of extended maxwell-garnett theories, Opt. Commun. **182**, 273 (2000).

[44] W. T. Doyle, Optical properties of a suspension of metal spheres, Phys. Rev. B **39**, 9852 (1989).

[45] H. Karl, J. Dreher, and B. Stritzker, Semiconductor-metal phase transition in doped ion beam synthesized VO_2 nanoclusters, MRS Online Proc. Library Arch. **1174**, 1174-V06-35 (2009).

[46] E. D. Palik, *Handbook of Optical Constants of Solids* (Academic Press, San Diego, CA, 1998).

[47] W. Rechberger, A. Hohenau, A. Leitner, J. Krenn, B. Lamprecht, and F. Aussenegg, Optical properties of two interacting gold nanoparticles, Opt. Commun. **220**, 137 (2003).

[48] P. Albella, M. A. Poyli, M. K. Schmidt, S. A. Maier, F. Moreno, J. J. Sáenz, and J. Aizpurua, Low-loss electric and magnetic field-enhanced spectroscopy with subwavelength silicon dimers, J. Phys. Chem. C **117**, 13573 (2013).

[49] S. Abdollahramezani, O. Hemmatyar, H. Taghinejad, A. Krasnok, Y. Kiarashinejad, M. Zandehshahvar, A. Alu, and A. Adibi, Tunable nanophotonics enabled by chalcogenide phase-change materials, arXiv:2001.06335 (2020).

[50] M. Kerker, D.-S. Wang, and C. Giles, Electromagnetic scattering by magnetic spheres, JOSA **73**, 765 (1983).

[51] W. Liu and Y. S. Kivshar, Generalized Kerker effects in nanophotonics and meta-optics, Opt. Express **26**, 13085 (2018).

[52] E. Rusak, J. Straubel, P. Gładysz, M. Göddel, A. Kędziorski, M. Kühn, F. Weigend, C. Rockstuhl, and K. Słowik, Tailoring the enhancement of and interference among higher order multipole transitions in molecules with a plasmonic nanoantenna, Nat. Commun. 10, 5775 (2019).

[53] J. D. Ryckman, K. A. Hallman, R. E. Marvel, R. F. Haglund, and S. M. Weiss, Ultra-compact silicon photonic devices reconfigured by an optically induced semiconductor-to-metal transition, Opt. Express **21**, 10753 (2013).

[54] P. Markov, R. E. Marvel, H. J. Conley, K. J. Miller, R. F. Haglund, Jr., and S. M. Weiss, Optically monitored electrical switching in VO_2, ACS Photonics **2**, 1175 (2015).

[55] Y. Gutierrez, D. Ortiz, J. M. Sanz, J. M. Saiz, F. Gonzalez, H. O. Everitt, and F. Moreno, How an oxide shell affects the ultraviolet plasmonic behavior of Ga, Mg, and Al nanostructures, Opt. Express **24**, 20621 (2016).

[56] T. W. H. Oates, M. Losurdo, S. Noda, and K. Hinrichs, The effect of atmospheric tarnishing on the optical and structural properties of silver nanoparticles, J. Phys. D: Appl. Phys. **46**, 145308 (2013).

[57] S. Cueff, F. Dubois, M. S. R. Huang, D. Li, R. Zia, X. Letartre, P. Viktorovitch, and H. S. Nguyen, Tailoring the local density of optical states and directionality of light emission by symmetry breaking, IEEE J. Sel. Topics Quantum Electron. **25**, 1 (2019).

[58] M. Decker, I. Staude, M. Falkner, J. Dominguez, D. N. Neshev, I. Brener, T. Pertsch, and Y. S. Kivshar, High-efficiency dielectric Huygens' surfaces, Adv. Opt. Mater. **3**, 813 (2015).

[59] H. Tompkins and E. A. Irene, *Handbook of Ellipsometry* (William Andrew, Norwich, NY, 2005).

[60] H. Fujiwara, J. Koh, P. Rovira, and R. Collins, Assessment of effective-medium theories in the analysis of nucleation and microscopic surface roughness evolution for semiconductor thin films, Phys. Rev. B **61**, 10832 (2000).

[61] A. Gavini and C. C. Kwan, Optical properties of semiconducting VO_2 films, Phys. Rev. B **5**, 3138 (1972).

[62] G. W. Mulholland, C. F. Bohren, and K. A. Fuller, Light scattering by agglomerates: Coupled electric and magnetic dipole method, Langmuir **10**, 2533 (1994).

[63] F. Moreno and F. Gonzales, *Light scattering from microstructures: lectures of the summer school of Laredo, University of Cantabria, held at Laredo, Spain, Sept. 11–13, 1998* (Springer Science & Business Media, Cantabria, Spain, 2000), Vol. 534.